INSA INSTITUT NATIONAL DES SCIENCES APPLIQUÉES LYON

Wing Experimentation and Simulation

CLARK-Y and NACA-0010 Aerofoil

Date: 12th January 2021

Jalendu Africawala

Emmanuelle Fried

Daniel Opoka

Professor : Ton Lubrecht

Table of Contents

Table of Figures

Table of Tables

1. Abstract

The report covers the fabrication process of a 90 cm long and 39.5 cm wide wing of the CLARK-Y aerofoil profile. Further, materials and tools used for the fabrication process have been elaborated. The assigned aerofoil for aerodynamic analysis was NACA 0010 which was achieved using an alternative software to X-foil called XFlr5. The bending strength of the rib was analysed using MATLAB and corroborated with RDM6 from which the stress distribution was studied. The torsional stiffness of the wing was tested and compared to an analytical model.

2. Introduction

There are many steps involved in the creation of a wing used by an aircraft as well as many materials used. Each was specifically chosen for a certain purpose due to their properties. In this report, the tools used for the building of a wing with a CLARK-Y aerofoil profile are explained as well as the materials for each section. The wing was made up of wing ribs, spars, leading edge and trailing edge covers, cap strips on the wing ribs and a skin that covered the whole wing. The wing itself was made up of many kinds of woods, for example samba was used for the individual wing ribs while spruce was used for the spars that connect all the wing ribs together. The only material that was not wood used for the wing was its skin, which was made up of nylon. This material is the same one used by gliders to make sure that there is no seepage of water into the wing as well as create a more aerodynamic surface throughout the whole wing.

XFLR-5 was used to study the aerodynamic performance of the NACA 0010 aerofoil profile. A standard study was done by utilizing a default chord length of 1 metre. The International Standard Atmosphere parameters for density, pressure and temperature were used. This first generic study gave an extensive understanding on the different relations the coefficients of lift and drag and the angle of attack have on each other in this configuration. Subsequently, the aerodynamic performance of a real-life application of this aerofoil profile was done by using the geometries of the wing used by the AVRO Canada CF100 Canuck.

Another object of study was an individual wing rib. The upper beam of a wing rib was modelled to be a cantilever beam, such that by recreating this mathematical model in MATLAB a series of forces could be obtained. By using RDM6, these assumptions were proven to be correct as the displacements obtained in the mathematical model and the computerised model of the software were one and the same. Two RDM6 models were made, one of the upper beam that bends into the shape of the wing rib and another of the rest of the wing rib composed of the trusses and the bottom beam. The forces obtained in MATLAB could be used on the two models to obtain their respective stress distributions.

During the building process of the wing, two kinds of test were done. One of them were bending tests, were the wing ribs bending stiffness was studied both experimentally and analytically. The other being torsional stiffness tests which were done on the different stages of assembly such as to have a better understanding of how specific components can greatly increase the structural integrity of the wing. This stiffness was studied both experimentally and analytically.

3. Materials

The section covers all the tools and materials that were used for the fabrication process. Moreover, a brief overview for the reason to use the specific material and certain tools for particular step is explained.

3.1 Tools

Hacksaw blade

The saw used to cut each type of wood was the blade of a hacksaw. This is a versatile blade, as it allowed for sawing of the small parts, such as the trusses for the rib, as well as for thicker parts, such as the spars. It is also a cheap, safe option that works well in the classroom environment.

Sandpaper

Sandpaper was used to finish any cutting that was too small to be done by the hacksaw, as well as smooth over joints between ribs and spars so that the nose and skin could be applied flush.

Rib Mould

The mould has two parts: a plastic plate with grooves that form the shape of the rib, and a backing with nobs placed so that, when pushed together with the plastic plate, the rib is pushed out at its nodes. This mould serves two functions: while one person assembles the rib with the plastic plate, another can use the backing as a miniature workbench. The mould is shown in Figure 1.

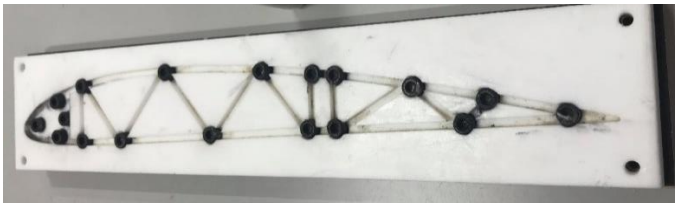

Figure 1: Rib mould

Ruler, meter stick

SI units. The meter stick was also used to check workplaces for flatness and levelness.

Plastic Covering

A plastic tarp was necessary to cover the workstation. Because the assembly was done in a classroom, it was imperative to respect the space.

Clamps

Clamps were particularly used at different stages of assembly that required the use of wood glue. An elastic band was used to secure the nose while the glue dried.

Pins

Pins were used to keep the plywood sheets in place while glue dries. In particular, these are used on the ribs when the plywood is added in the form of caps trips on both the top and bottom of the rib.

Iron

An iron was used to heat the skin. It has three heat settings. The 2nd and 3rd were used.

3.2 Building Materials

Since the wing fabrication process was carried out in France, all the wood used is of European origin. This is mainly for availability and economical purposes.

Samba

Samba is the wood used to build the ribs. This wood is flexible but strong. These properties are essential for the rib because the wood is bent into shape and must be able to remain elastic during deformation. Its young modulus is 6.69 GPa. It is strong, yet light. On the left side of Figure 2, the ribs made of samba are shown.

Spruce

Spruce is used for the spars that connect the ribs. Its Young's modulus is 71 MPa which is much higher when compared to samba, resulting, in higher bending and torsional stiffness.

Balsa

Balsa was used as webbing between spars. It is extremely light and very strong when in tension across the grain, but not when bent or pulled along the grain. It was therefore important to take care to cut and assemble the webbing with the grain in the vertical direction. The Young's modulus of balsa was taken to be 183.6 MPa.

Plywood

The final wood used was plywood. A very thin sheets used to cover the nose, trailing edge, and the ribs. This would not only increase torsional stiffness, moreover the thin sheets created a smoother, more aerodynamic surface.

Wing Skin

The final step in building the wing was to cover it with a nylon skin, the same type used on gliders. This skin is thermally activated. When heat is applied, two things happen: the adhesive backing is melted just enough to create a bond with the wood, and the skin itself shrinks.

Super Glue

Super glue was used as the adhesive for the ribs as well as between the spars and the ribs. This glue is activated by moisture and therefore dries very quickly. Hence, the intent of using super glue was for the building steps that demanded quick actions.

Wood Glue

The wood glue was used in joints that needed a stronger bond without a constraint on drying time. Therefore, the wood glue was used in the joints of balsa webbing and spars, plywood trailing edge and samba ribs, plywood sheets and samba ribs. When this glue is used, clamps, elastic bands or pins must be used to keep the two pieces of wood in place during the drying time.

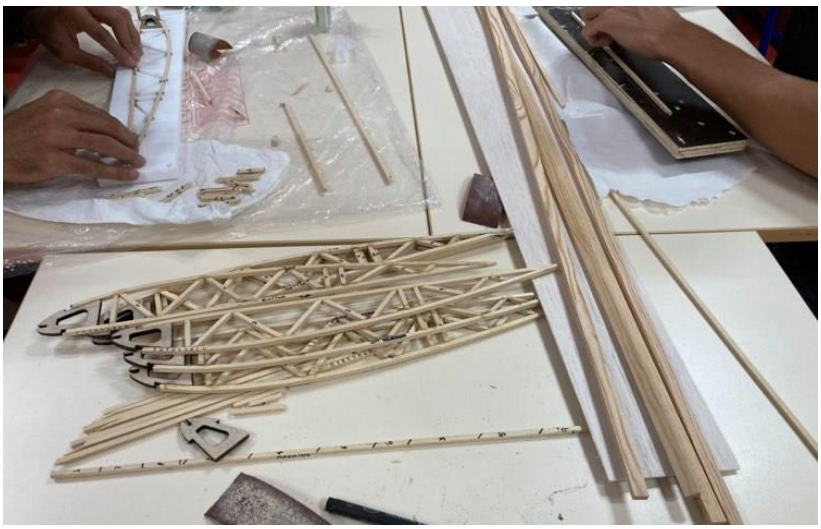

Figure 2: Ribs made of samba and spars made of spruce

4. Wing fabrication procedure

This section of the report elaborates the building process in a progressive manner. Building of a wing is a tedious process and demands patience as some steps require more time in order to attain perfection.

4.1 Building ribs

The first step in building the wing started with construction of eleven ribs. To do so, wooden sticks of dimension 4x4 mm, made of samba, were sawed to fit in the mould in Figure 1. At first, the laser-cut nose of the rib was placed in the mould. Top and then bottom of the wooden sticks were bent to fit in the mould. A gap of about 5 mm was left between the nose and edge of the top and bottom sticks. The dimensions of each truss beam were marked onto a standard stick so that measuring and cutting could be done quickly. Once all the wooden pieces were set in the mould, super glue was used to stick them together. Small dots of glue were sufficient for the durable adhesion of the samba pieces. The glue dries hard. The nobs on the backing were used to push the rib out of the mould through the holes on the back of the mould. This process was repeated to make remaining ten ribs.

4.2 Connecting ribs using spars

Once all the ribs were built, ten of them were used to continue with the wing fabrication. These ribs were then spaced equidistantly to achieve the preliminary shape of the wing. Spars made of spruce were inserted within the ribs in spaces at the front and back made specifically to fit the spars. This process required a lot of strength and needed at least two people, since the spars are inserted vertically and have to be turned horizontally to achieve a tight fit. However, the spars were turned only after the ribs were spaced equidistantly. Then, the ribs were super-glued to the spars. When doing so, it was necessary to make sure that the spars were pushed completely towards the top or the bottom of the rib respectively, depending on which spar was being installed. This process was repeated for two spars in the front, top and bottom of the spacing as well as for the back. Figure 3 shows the wing after completing the procedures mentioned above.

Figure 3: Ribs connected using spars

4.3 Webbing with Balsa

After connecting the ribs with the spars, the next step was to add webbing between the spars to increase the torsional stiffness of the wing. Balsa was the wood used for this purpose. The balsa webbing is illustrated in the Figure 4: it is the thin sheet of wood clamped to the spruce spars while the glue dries. As explained in section 3.2, balsa has more stiffness under tension along the direction of the grains, hence it was attached so that the grains run vertically, perpendicular to the spars. Balsa was glued on the inner and outer surface of each pair of spars. Since time was not a constraint in this situation, wood glue was used to attach the balsa. This provides stronger bonding between the balsa and the spars. Since wood glue requires approximately 30 mins to dry, clamps were used to keep them in place. These clamps also made sure that the balsa was evenly adhering.

At first, the webbing was only added to the spars at the extremities of the wing and was then tested to get a preliminary torsional stiffness measurement. The remaining parts were webbed, and the actual test was performed to observe how the torsional stiffness had increased drastically when the webbing was added.

Figure 4: Balsa webbing being glued onto the spars

4.4 Adding covers at the leading and trailing edge

After webbing, the next step was to add tapered support to the trailing edge. The support is made from balsa that is attached between the ribs. The support pieces used were already tapered and had to be cut to size to fit between the ribs.

Figure 5: Trailing edge support

Similarly, a thin spruce strip had to be inserted inside the groove at the nose tip, the leading edge of the wing. Additionally, the gap left between the nose and top samba beam, as mentioned in rib fabrication section 4.1, had to be filled with a 4x4mm samba stick running horizontally. Wood glue was used to attach these supports at the leading and trailing edge. Then, pre-bent plywood was used to cover the nose. Plywood was also added to the trailing edge. It was initially attached using wood glue and then it was tightly wrapped with long elastic bands to avoid air bubbles and to ensure perfect sealing. In addition, long plywood was glued to the top and the bottom of the trailing edge. While the wood glue dried, pins were used to secure the plywood in the required position. Figure 6 presents how the wing looks after these steps were completed.

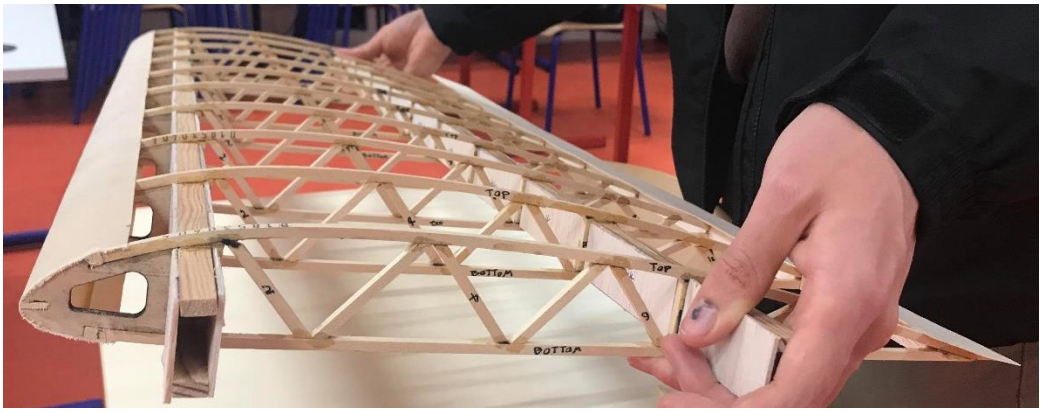

Figure 6: Wing with nose cover and plywood at the trailing edge

4.5 Attaching cap strips to the ribs

The second to last step was to attach cap strips made of plywood to the top and the bottom of the ribs. These strips of plywood were attached using wood glue and then secured using pins while the glue dried. Moreover, the cap strips provided an even surface flushed with the leading and trailing edge covers. When tested, a significant increase in torsional stiffness was observed.

4.6 Covering wing with skin

The final step of the wing fabrication was to cover it with nylon skin. The skin was cut to size for the top and the bottom. Once the glue protection paper was removed, the skin was laid onto the wing and ironed. The skin was preliminarily heated with an iron on a low setting in order to just melt the backing so that the skin would adhere to the wing. Once the skin was secured, the iron was set to a higher temperature and the skin was shrunk in order to remove any wrinkles and to create a tight-fitting layer. The nylon was added so that its fibres ran vertically from front to back, which allowed for horizontal shrinkage. This orientation helped to increase torsional stiffness of the wing. Once the skin had shrunk to fit, the extra nylon on the outer side of the wing was cut using razor blade. The top skin had to just overlap the bottom to prevent water seepage.

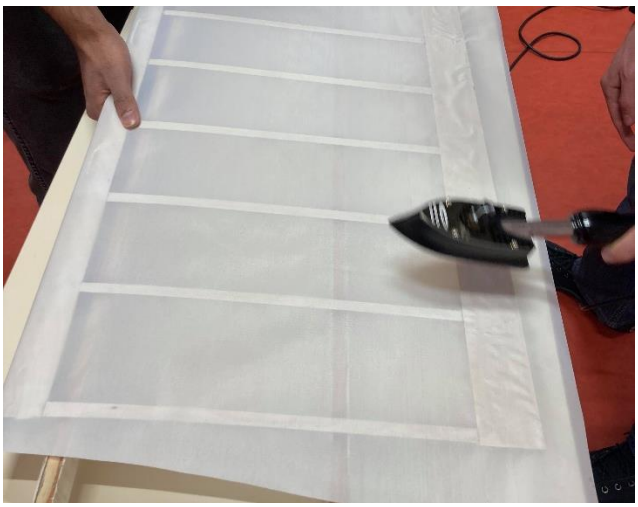

Figure 7: Ironing the skin to adhere

5. Measurements

At multiple stages during the fabrication process torsional stiffness tests for the wing and bending tests for the rib were performed. These tests helped to quantify the strengthening processes for wings. In addition, the measurements collected for these tests were later compared with analytical results, which determined the accuracy of experimental tests and how the performance of the wing measured up to the mathematical model proposed.

5.1 Bending stiffness of a wing rib

To test the bending stiffness of a rib, the rib was laid across two tables so that a weight could be hung from the middle in between the tables. The vertical deflection was determined by measuring the distance between the deflected rib and a straight ruler placed on the rib. This was done for a plane rib, and then when the cap-strips were applied.

Figure 8: Bending stiffness of rib with cap-strip measured using water bottle

With the value of the weight and the resulting vertical deflection, the bending stiffness is found using:

$$k = \frac{P}{w}$$

Where P is the force applied and w the vertical deflection.

The measurements found in both tests are given in Table 1.

Table 1: Results of bending stiffness tests

	Weight (in N)	**Deflection (in cm)**	**Bending stiffness (in Nm)**
Plane rib	4.9	1.2	409
Rib with cap-strips	9.8	0.4	2450

5.1 Torsional stiffness tests

Torsional stiffness was measured at each stage of assembly in order to study the effect of each stage on the strength of the wing. In order to measure the torsional stiffness, the wing was fit between two aluminium L-shaped bases to which were the attached wooden plates with the marking to fit the spars. On the wooden plates were four protrusions that secured the spars of the wing in between. As it can be seen in Figure 9, one of stands had an iron rod to which a jockey weight would be added in order to test the wing under a given moment. The wing was always tested under clockwise moment motion to mimic a real-life scenario. The weight was adjusted until the metallic rod was parallel to the ground. Then, the distance from the centre of moment to the centre of the weight was measured.

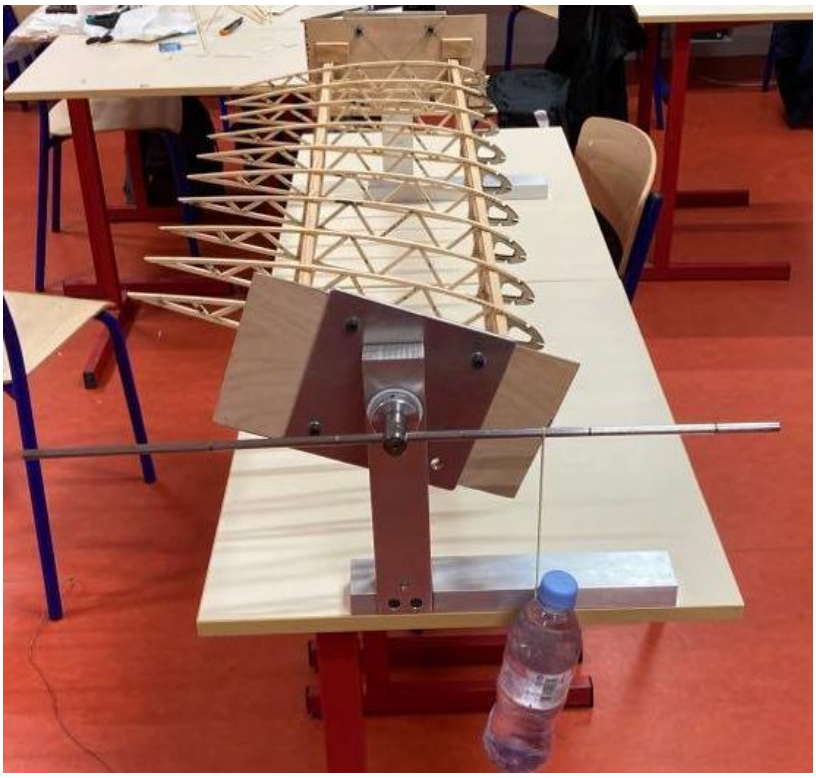

Figure 9: Illustration of torsional stiffness test

This is how the stages are defined for the torsional stiffness test:

First Stage: The first stage of construction consists of just the spruce spars connecting the ten ribs with balsa webbing at just the 4 extremities.

Second Stage: The second stage of construction consists of balsa webbing added between the spars.

Third Stage: The third stage of construction consists of adding plywood to the nose and trailing edge.

Fourth Stage: The fourth stage consists of adding cap-strips to the top and bottom of each rib.

Fifth Stage: The fifth and final stage consists of adding the skin to the wing.

The moment produced by the iron rod's weight was only taken into account in the measurements when its centre of gravity was not in the central axis of torsion at the centre of moment; this only happened for the fourth and fifth stage. The rod's density was assumed to be that of a generic steel. Annex 8.2 outlines the dimensions of the rod and the resulting torque due to its mass.

The torque was calculated by multiplying the weight applied to the rod by the distance where the weight must be placed to make the rod parallel to the ground. Using the torque applied to the wing, the experimental torsional stiffness was determined using:

$$k = \frac{T}{\emptyset}$$

Where T is the torque and $\emptyset$ is the torsion angle.

Table 2 presents the results of the experimental torsional stiffness tests for each stage.

Table 2: Experimental results of torsional tests

Stage	Weight (in N)	Distance (in cm)	Moment (in Nm)	Torsional stiffness (in Nm)
1st	4.9	12	0.58	1.9
2nd	14.7	13.5	2.0	6.3
3rd	9.8	30.5	3.0	9.5
4th	9.8	32	3.8	12.2
5th	9.8	33.5	4.0	12.7

6. Analysis

Three forms of analysis were performed in this project. First, the aerodynamic performance of aerofoil NACA 0010 was studied using XFlr5. Then, the forces within the rib were analysed using RDM6 and MATLAB. Finally, mathematical models were compared to the results found in the bending and torsional stiffness tests.

6.1 XFlr5

The aerodynamic performance of the NACA 0010 aerofoil was analysed. NACA 0010 is a symmetrical aerofoil, meaning it creates lift with both positive and negative angles of attack. However, it is known to stall at a much lower angle of attack when compared to an asymmetrical aerofoil. These traits of the aerofoil make it particularly interesting for aircrafts used for dog fights where quick manoeuvres are necessary. One of the aircrafts that used the NACA 0010 aerofoil is the AVRO Canada CF100 Canuck used in 1950s. It is a Canadian twinjet interceptor/fighter aircraft and the only known Canadian fighter-jet to undergo mass production. Further analysis for this aircraft has been performed. [1]

6.1.1 Standard NACA 0010 analysis

The standard aerodynamic analysis consists of neglecting all the geometrical factors and using the standard aerofoil chord length, 1 metre. The only parameter that is varied is the Reynolds number.

Moreover, even the atmospheric parameters like density and kinematic viscosity can be kept at International Standard Atmosphere (ISA). Below are the ISA values used.

$$\rho = 1.225\,\frac{kg}{m^3},\ Pressure = 101325\ Pa,\ and\ Temperature = 288.16\ K.$$

Here the standard NACA 0010 analysis was done at two different Reynolds numbers: 50,000 and 1,000,000. Reynolds number is expressed as

$$Re = \frac{\rho \cdot L \cdot v}{\mu}$$

Where ρ, the density, L, the characteristic length, or chord length, and μ, the dynamic viscosity, are constant. v, the veolicty, is the only variable.

Figure 10 highlights the various graphs of coefficient of lift, CL, and Coefficient of drag, CD. The top left graph represents change in coefficient of drag with coefficient of lift. The top right and bottom left graph plot CL and CD versus change in angle of attack respectively. The last graph plots CL/CD with change in angle of attack. The blue line represents values with a Reynolds number of 50,000 whereas the magneta line represents a Reynolds number of 1,000,000.

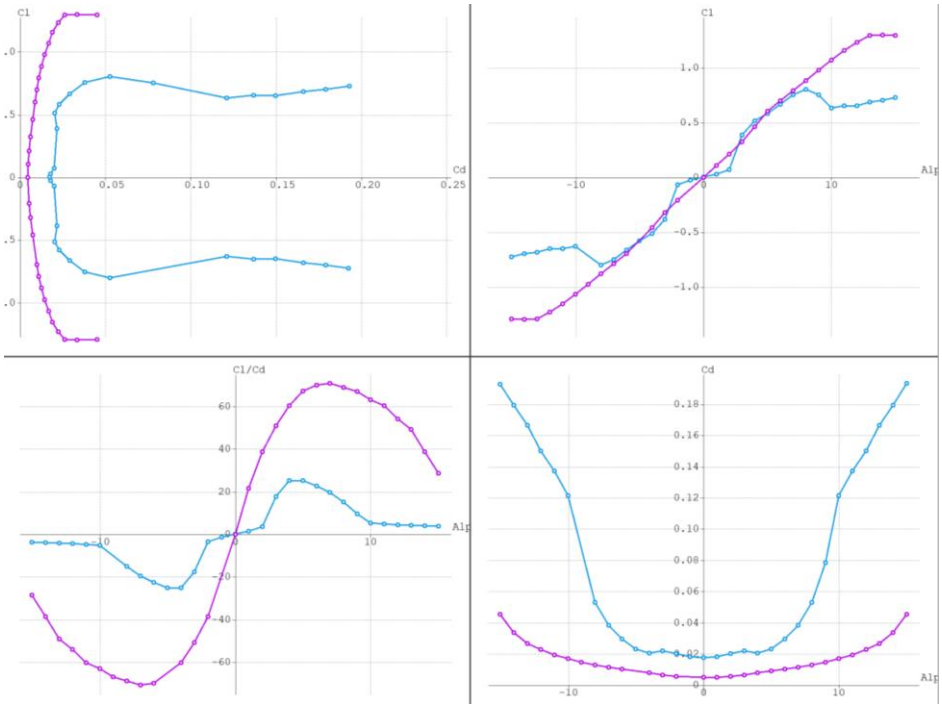

Figure 10: Standard NACA 0010 analysis

The CL vs alpha and CD vs alpha graphs show symmetry when change in alpha is positive or negative. The stalling angle at Re=50,000 can be noticed to be about 8 degrees, whereas it is about 14 degrees for Re=1,000,000. Although it can be seen to have an increase in CL again after stall, the coefficient of lift cannot surpass the maximum achieved at the stalling angle. The symmetry between positive and negative angles of attack in graphs for coefficient of lift and drag confirms the manoeuvring trait of symmetric aerofoils.

6.1.2 AVRO Canada CF100 Canuck aerodynamic analysis

A different aerodynamic analysis was performed that corresponds to an aircraft in level flight at a given altitude undergoing trim speed changes [2]. The geometrical dimensions that were necessary in order to accomplish this analysis are given in Table 3.

Table 3: Geometric dimension needed for trim analysis [1]

Geometrical Dimension	Value
Chord Length	4.24 m
Wingspan	16 m
Wing Area	54.9 m^2
Gross Weight	15000 kg

This analysis was performed at sea level as well as service ceiling, which is at 14 km of altitude. While analysing an actual wing, it is important to use $Re \cdot \sqrt{CL}$. This ensures simplification by removing the variable which is velocity from the equation. As $Re = \rho \cdot L \cdot v/\mu$, and $Cl = \frac{2 \cdot W}{A \cdot \rho \cdot v^2}$.

$$\therefore Re \cdot \sqrt{Cl} = \frac{L}{\mu}\sqrt{\frac{2 \cdot \rho \cdot W}{A}}$$

When $Re \cdot \sqrt{CL}$ is constant, we can determine the Re needed to achieve maximum climb performance, owning to trim in climb velocity.

Annex 8.5 outlines the analysis toolbox and the variables used to achieve the aircraft performance at sea-level.

At sea level

Figure 11 presents the resulting graphs with the data presented.

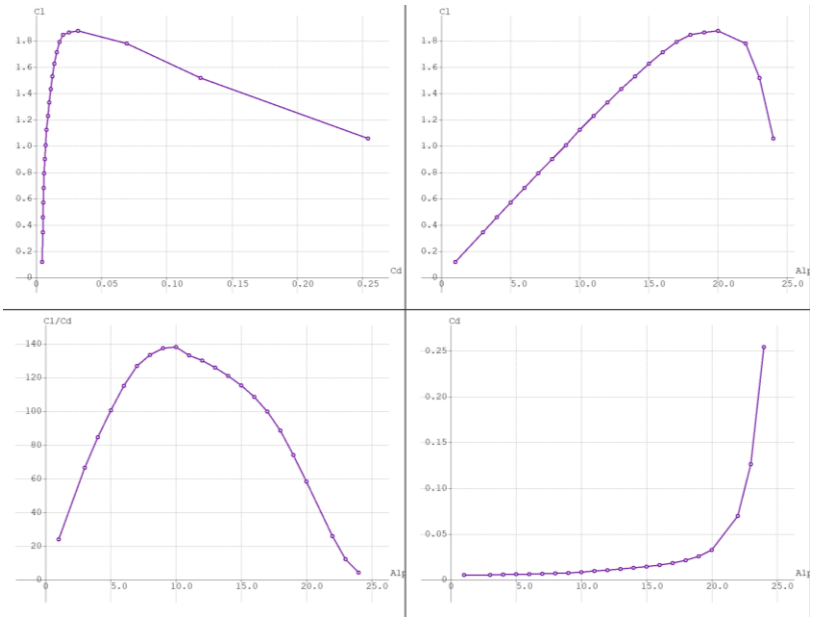

Figure 11: Graphs of aerodynamic coefficients at sea level

It can be observed from Figure 11 that the aircraft stalls at 20°. However, the maximum CL/CD is at approximately 10°. Moreover, the CL vs CD graph, top left, shows that the coefficient of drag is almost negligible until the maximum coefficient of lift is obtained.

In additon, coefficient of pressure, CP vs x, dimensionless length, is represented in Figure 12. This graph was plotted at 20° to observe the pressure distribution along the wing when the aircraft stalls. We can visually check the high intensity of the CP at the nose which almost completely diminishes by the end of trailing edge. Moreover, flow seperation can be seen over the aerofoil represented by the red dotted line. The flow is observed to separate at nearly half of the chord. The Re corresponding to maximum climb is 12,268,000, from which velocity can be achieved using the formula $Re = \rho \cdot L \cdot v/\mu$. Velocity of maximum climb performance at sea level is 42.5 m/s.

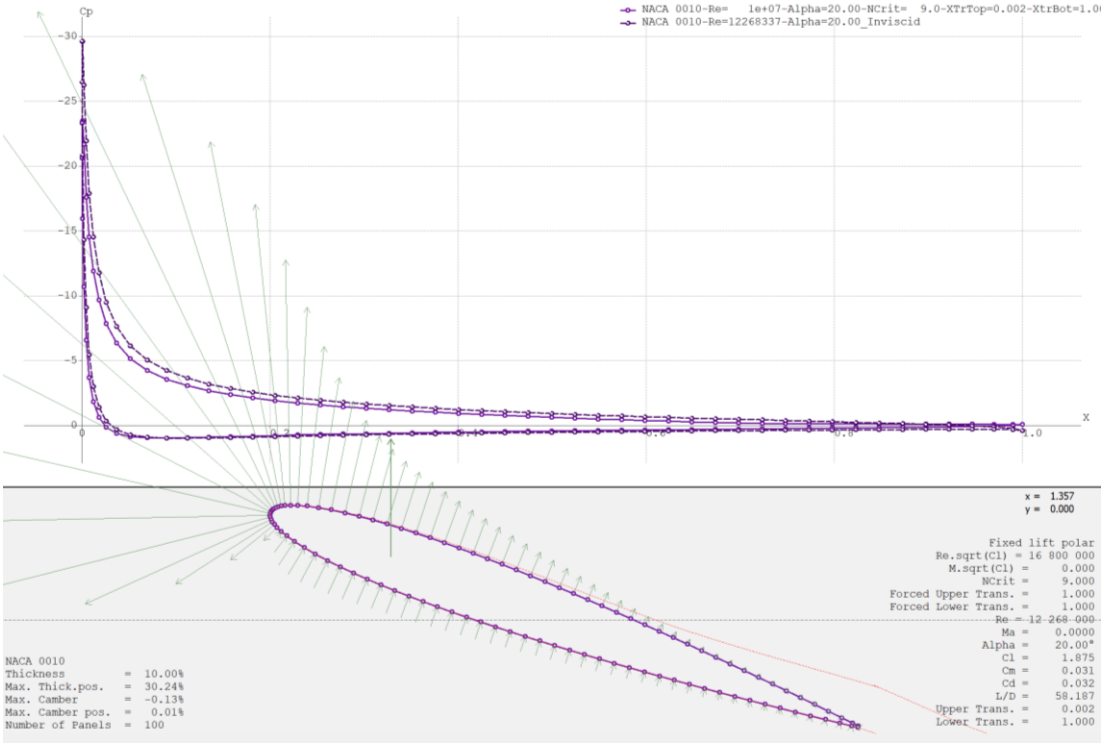

Figure 12: Cp vs x/c, dimensionless length, and flow separation at stall angle at sea level

At service ceiling (14 km altitude)

With all the data entered to achieve the aerodynamic performance, the graphs presented in Figure 13 are produced for flight at 14km altitude.

It can be observed from Figure 13 that the stalling angle is approximately 18°, where CL is 1.8, which is about 10 percent lower than that at sea level. Moreover, CD surges only after stalling.

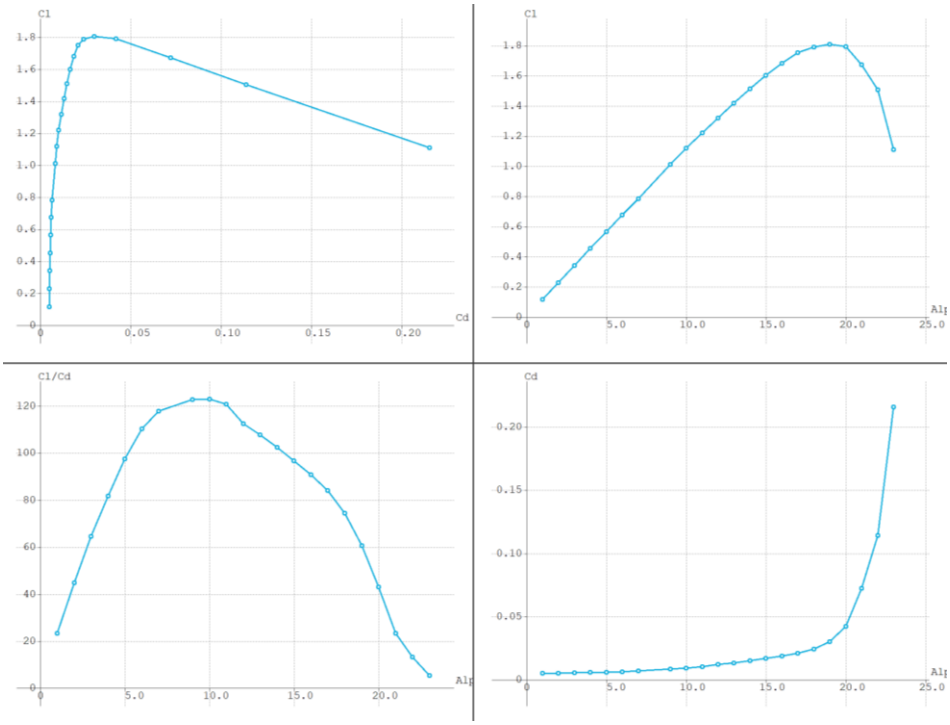

Figure 13: Graphs of aerodynamic coefficients at service ceiling

Figure 14 illustrates CP vs x at 18°, when the aircraft stalls at the altitude of 14km. Again, the flow separation occurs at about half of the chord length. The Re at the maximum climbing performance is 6,980,000, from which the velocity corresponding to max climb is 102.35 m/s.

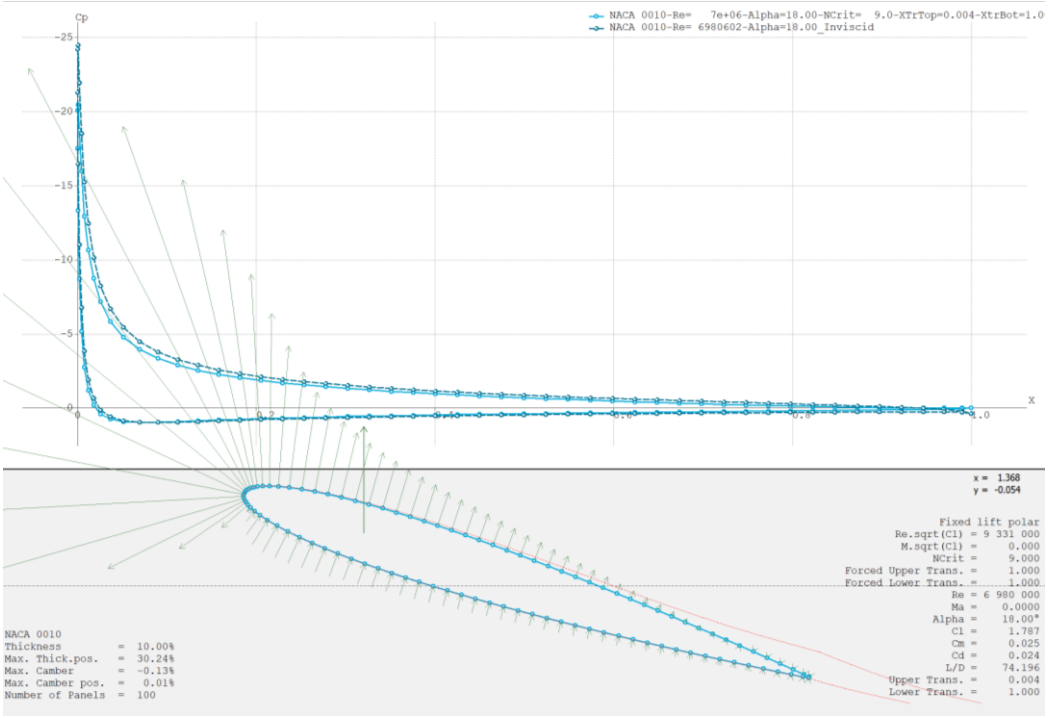

Figure 14: Cp vs x/c, dimensionless length, and flow separation at stall angle at service ceiling

6.2 RDM6

To study the wing rib as it comes out of the mould, the following were created: (1) reference frames based on geometrical assumptions, (2) calculations of displacements for future modelling, (3) cantilever beam modelling to obtain the forces needed to bend a straight beam into the wing rib shape and (4) the study of the stress distributions caused by these forces.

Only the upper beam of the wing rib will be studied; however, the effects of the trusses will be modelled as compression or tension forces. A .dat file containing the coordinates for 122 points needed to recreate the CLARK Y aerofoil was obtained [3]. Only the first 61 coordinates of the .dat file will be considered as they represent the upper beam of the wing rib. The file creates an aerofoil of length 1. To convert them to the rib studied, they were all multiplied by 39.5 cm, the measured length of the wing rib from tip to tip. Before modelling the upper beam, the coordinates of where the trusses connect to the beam were obtained. These are the foundation of future calculations. To accomplish this, a real-life scale drawing of the wing rib was made. Both the drawing and the truss intersection points are outlined in annex 8.6 as Figure 24 and Table 8 respectively.

6.2.1 Reference frames

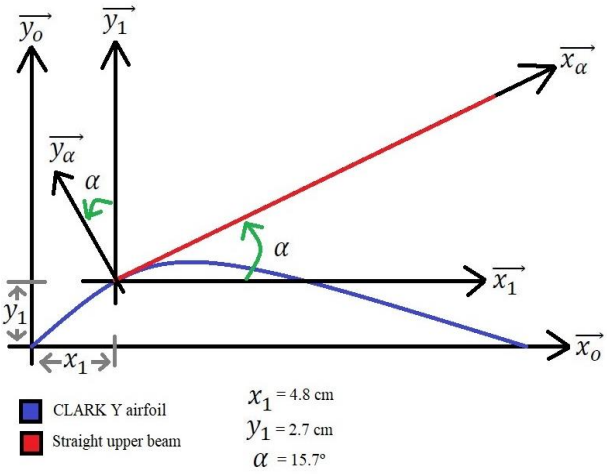

Figure 15: Reference frames of the wing rib

Reference frame 0 (RF0) represents the x-y directions considering the leading nose tip of the wing rib as the origin. Reference frame 1 (RF1) represents the same x-y directions of the previous frame however they are displaced by an x offset of 4.8 cm and a y offset of 2.7 cm. These points are where the straight upper beam will be bent to form the shape of the wing rib. The reference frame α (RFα) is created by rotating RF1 in a counter-clockwise manner by α=15.7º. This angle is the last one formed by the last two points where the offset to form RF1 occurs. The calculations of this angle are outlined in annex 8.6 as Figure 25 .

6.2.2 Displacement calculations

The points where the trusses intersect the upper beam will be known as the truss intersection points (TIP). These points are located on the beam as if it were straight in the direction. They are known

as the Straight Upper Beam Points (SUBP). These points can be obtained by using the Pythagorean theorem of two successive coordinates of the TIPs and adding the previous value obtained as shown in annex 8.6 as Figure 26. The points are in the $\overrightarrow{x_\alpha}$ direction, therefore they can be transposed into RF1. The distance between each TIP on the CLARK Y aerofoil coordinates and the SUBPs will be known as Δy and is in the $\overrightarrow{y_1}$ direction; this displacement is needed to understand how much distance the straight beam has to deflect in the $\overrightarrow{y_1}$ direction such that the wing rib shape is achieved. The values obtained for the TIPs, SUBPs and δ_{y1-8}, are in annex 8.6 as Table 9.

6.2.3 Cantilever beam modelling

The beam will be submitted to 8 different forces (which are unknown) called $F_{1\text{-}8}$ that will act in the $\overrightarrow{y_\alpha}$ direction at the SUBP coordinates. The distance of δ_{y1-8} must be translated to the $\overrightarrow{y_\alpha}$ direction such that it can be correctly used in the following model. The deflection produced by bending the straight beam must equal to δ_{y1-8}. The deflection caused by these forces can be calculated by using the equations for the deflection of a cantilever beam caused by a perpendicular force to the beam shown in Figure 16.

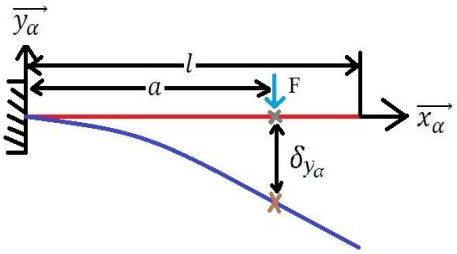

$$For\ 0 < x < a: \delta_{y\alpha,1-8} = \frac{F_{1-8} \cdot x^2}{6 \cdot E \cdot I}(3 \cdot a - x)$$

$$For\ a < x < l: \delta_{y\alpha,1-8} = \frac{F_{1-8} \cdot a^2}{6 \cdot E \cdot I}(3 \cdot x - a)$$

$$For\ x = l: \delta_{y\alpha,1-8} = \frac{F_{1-8} \cdot l^3}{3 \cdot E \cdot I}$$

Figure 16: Beam Deflection formulae [4]

E is the Young's modulus of the material and I the second moment of inertia of the geometry of the beam. The deflection is already known in the $\overrightarrow{y_\alpha}$ direction, as this would-be δ_{y1-8}. However, to account for the eight unknown forces and their respective displacements, a superposition of all of these had to be made. An illustration of this is shown in Figure 17.

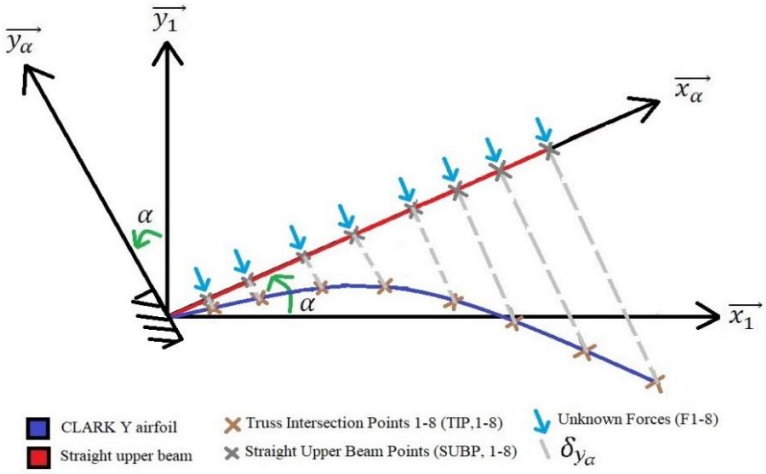

Figure 17: Illustration of cantilever beam deflection with 8 unknown forces

An unknown force that will be considered a variable will be placed at its respective SUBP and the deflection this force induces will be calculated for not only where the force is applied, but also to the remaining seven points. After creating all 8 scenarios and leaving the forces as unknowns to later be calculated, 64 values are obtained. The addition of all the displacements caused by the eight forces on one point must equal to the δ_y of that point. All lengths were converted to meters so it could be used in the cantilever beam equations. Mathematically, this physical circumstance can be represented as the following 8 by 8 matrix shown in annex 8.6 as Figure 27.

As this 8 by 8 matrix assumption will result in 8 unknowns and 8 equations, it can be solved.

To facilitate this arduous task, MATLAB code was utilized to recreate the previously described steps. First, eight unknowns that are kept as variables are made using the syms function to create symbolic variables. Secondly, the matrix was created by using a nested for loop such that each force and each SUBP is considered, then an equation where the addition of each the contributions of the 8 unknown forces equals the known 8 values of the δ_y displacement is created such that a system of equations can be solved. Finally, the solve function was used to obtain all the unknowns. This code is called CLARKY_WINGRIB_CALCULATIONS and it will be attached as a .mat file with this report, additionally an .xls file containing the CLARK Y aerofoil coordinates will be attached such that the MATLAB code can work. The resulting forces are outlined in annex 8.6 in Table 10.

To corroborate this information, the results obtained from the MATLAB code will be compared to an RDM6 model. This model will have the values of F in the x1 and y1 direction placed on its respective SUBP with the origin (the origin of Reference frame 1) as a clamped support. The material properties used in RDM6 are given in annex 8.1.

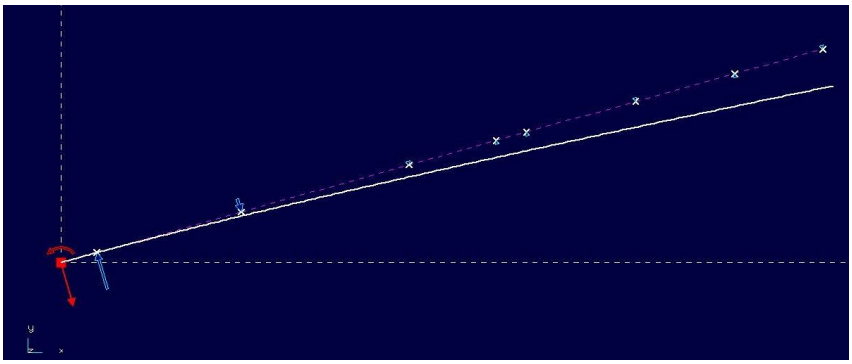

Figure 18: RDM6 model of upper beam

After the software analysed the beam subjected to the given forces obtained from the code, the displacements, dy from the results of the analysis will be considered as the real values which the MATLAB code was supposed to obtain. RDM6's results of this model for the displacements are relative to RF1, where the values for dy are in the $\overrightarrow{y_1}$ direction. A percent error between the RDM6 results and the MATLAB code was done to compare the two, where the δ_{y1-8} are considered the measured values and the RDM6's dy the real values. A table containing both results and the error are outlined in annex 8.6 as Table 10.

The average percentage error is 0.034 % and the largest error is of 0.098 millimetres on the final, eighth node. Therefore, the mathematical and physical assumptions made by representing this situation as a superposition of 8 different cantilever beam deflections was correct. The theory was corroborated with the RDM6 software as there was no great error to be found between the analytical values, δ_y and the experimental values, dy.

6.2.4 Study of stress distributions

These are the following results obtained from the stress distributions from the upper beam RDM6 model. Since there were no forces applied on the $\overrightarrow{x_\alpha}$ direction on the straight upper beam, there was no normal stress induced unto the beam. All the forces applied were perpendicular to the beam, thus shear stress was produced with the highest stress occurring in the second node. A force of 19.625 N in the $\overrightarrow{y_\alpha}$ direction was applied to the first node of the upper beam resulting in a maximum shear force of 11.62 N. The highest bending moment happened in the same place with a maximum of 72.26 N.cm. As expected, this node suffered the highest stress of 67.74 MPa calculated from the addition of the bending moment and the normal stress.

To study the rest of the wing rib, a RDM6 model of trusses along with the bottom beam was made. The forces previously obtained, which are needed to bend the upper beam in the shape of the wing rib, are considered and placed in the opposite direction due to the action reaction principle. The locations where the trusses intersect the bottom beam are assumed to be the ground of this system such that the displacements of the trusses and the end of the wing rib can be studied. Figure 19 represent the RDM6 model just explained.

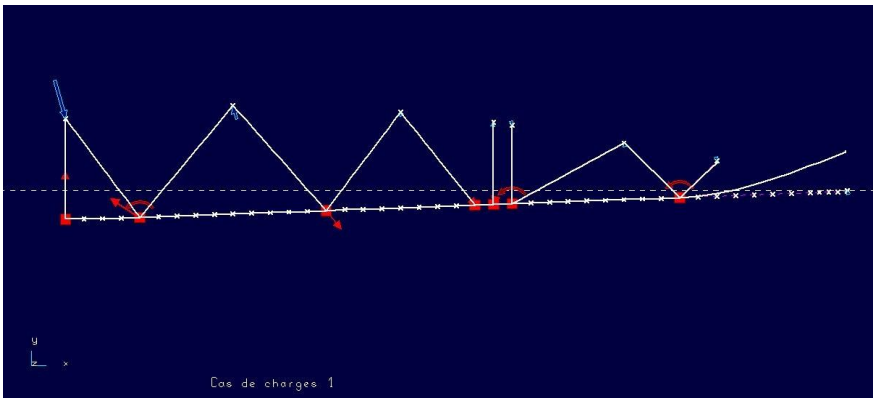

Figure 19: RDM6 model of trusses under the forces from the upper beam

The trusses suffer no substantial deflection however the end of wing rib does with a maximum deflection of +0.012 cm in the $\overrightarrow{x_0}$ direction and +0.256 cm in the $\overrightarrow{y_0}$ direction. In node 1, the leftmost truss, there is a maximum normal force of 11.85 N due to the highest force for bending the upper beam of 19.625 N. Due to the assumption of considering the intersection of the trusses with the bottom as being the ground, most of the forces are now considered as reaction forces and moments instead of deflections; this results in the maximum reaction force being 11.8 N on the first (leftmost) ground support node which is the result of the highest normal force. The highest reaction moment is in node 34 (the final ground support before the free end) of -14.5 N.cm, as

expected the highest bending moment is of 21.67 N.cm and the modulus of normal stress is of 20.36 MPa at this location.

6.3 Stiffness

The overall performance of the wing was evaluated in part by the stiffness of both a rib and of the wing.

6.3.1 Bending Stiffness

With the value of the weight and the resulting vertical deflection, the bending stiffness is found using $k = \frac{P}{w}$ where P is the force applied and w is the vertical deflection.

The results for both measurements are given in Table 1 in section 5.1.

Comparison with stiffness of one beam

One measure of the efficacy of the rib, is to compare its stiffness to that of a samba beam used in the rib. The bending stiffness of one beam is calculated using $k = \frac{IE}{L}$ where I is the moment of inertia, E is the Young's modulus, and L is the length of the rib.

There are two orientations to consider when adding beams together to achieve equivalent stiffness, side-by-side, or stacked vertically. Considering the equivalent beams to be placed side-by-side is similar to the actual situation in the rib where the top and bottom beams are essentially side by side when the rib is laid on the table. If the equivalent beams are considered to be staked vertically, the resulting structure will better resist vertical bending, but this situation does not correspond to a possible real orientation. The explanation of how the equivalent number of beams were calculated, both in the horizontal and vertical alignment, are explained in Annex 8.3.1 and 0.

The results are outlined in Table 4. As predicted, stacking beams vertically results in a stronger structure and less material is needed. As shown, the rib with cap-strips is six times stronger than the rib without cap-strips. To achieve the same stiffness as a rib with cap-strips, almost 13 beams would need to be aligned side-by-side. This shows that cap-strips are an extremely efficient and effective way to increase rib strength.

Table 4: Bending Stiffness Results

	K (Nm)	Equivalent number of beams, side by side	Equivalent number of beams, stacked vertically
Without Cap-strip	409	2.1	1.3
With Cap-strip	2450	12.9	2.3

6.3.2 Torsional Stiffness

For the first three stages, the torsional stiffness found experimentally was compared with the torsional stiffness found analytically.

Using the torque applied to the wing, the experimental torsional stiffness was determined using

$$k = \frac{T}{\emptyset}$$

From here, the analytical torsional stiffness can be determined using $\emptyset = \frac{TL}{JG}$. Therefore, $k = \frac{JG}{L}$ where $J = I_x + I_y$.

The values of the shear modulus for each material can be found in Annex 8.1 while the full calculations of the torsional moment of inertia, analytical torsional stiffness and analytical torsion angle for each component at each stage can be found in Annex 8.2. Table 5 outlines the results produced both experimentally and analytically. As seen in the third stage, the percent error is negative. This is because the material added to the trailing edge was ignored, which resulted in a less stiff model.

Table 5: Torsional Stiffness Results

	Analytical Torsion Angle (rad)	Analytical Torsional Stiffness	Experimental Torsional Stiffness	Percent Error between Analytical and Experimental Torsional Stiffness
1st Stage	0.26	2.3	1.9	20.3%
2nd Stage	0.39	6.9	6.3	9.3%
3rd Stage	0.18	9.3	9.5	-2.3%
4th Stage	----	----	12.2	----
5th Stage	----	----	12.7	----

As shown in Figure 20, the greatest increase of torsional stiffness occurs at stage 2 when the webbing is added. This is a testament to the efficacy of the webbing in increasing torsional strength.

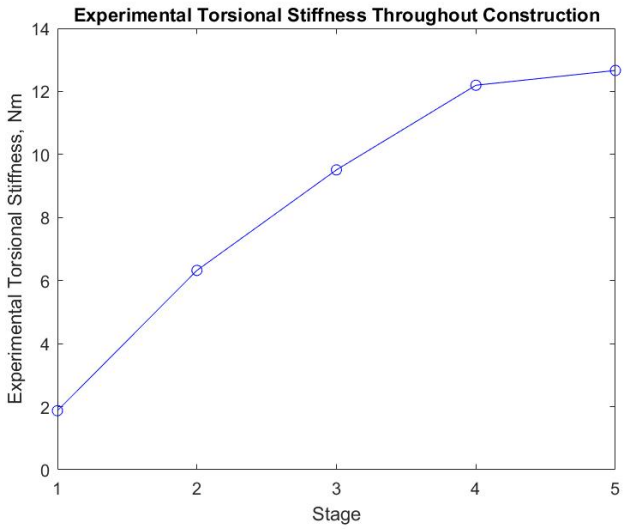

Figure 20: Plot of the experimental torsional stiffness of wing throughout construction

7. Conclusion

The processes of building and testing this wing protype provides a clear idea of the importance material properties play in maximising wing strength. Indeed, maximising strength does not always mean a compromise in weight. This processes also illustrated the precision and time needed to build a perfect wing. In addition, the bending and torsional tests performed correspond to the tests an actual wing undergoes.

The preliminary analysis performed on the NACA 0010 aerofoil studied the characteristics of this type of an aerofoil. However, to further understand the aerodynamical analysis on a wing, a particular examination was performed for the wing of AVRO Canada CF100 Canuck that utilised NACA 0010 aerofoil. In order to perform this in depth aerodynamical analysis, all of the geometrical parameters on the aircraft's wing were found. These geometrical parameters, chord length, wingspan, wing area, and load on the wing were used along with $Re \cdot \sqrt{CL}$ as inputs and formula to analyse the maximum lift in a levelled flight. This resulted in understanding that at different altitudes, trim in velocities is needed to achieve the max lift, which was about 40m/s at sea level and 100m/s at the ceiling level. Hence, the maximum lift at an altitude did not at all correspond to the cruising speed or the maximum speed of an aircraft.

The assumption of modelling the upper beam of the wing rib as a cantilever beam has been corroborated with RDM6 to demonstrate its validity. This shows that through modelling, a better understanding of the object is obtained. The study of stress distributions within the rib illustrate the physical phenomena the wing rib is under to maintain the shape it has. The maximum stress found in the upper beam, according to its RDM6 model, indicates that the stress induced is higher than the yield strength of the material it is made of. The beam is no longer in a plastic state from which it can revert to its original configuration and is permanently deformed to become the wing rib.

Finally, the results obtained in bending and torsional tests prove the efficacy of each step conducted in the building process. Adding webbing between spars triples torsional strength, while adding cap strips multiplies bending stiffness by six. Additionally, the mathematical model proposed fits very closely with the experimental results obtained in the lab. This shows that the equations used and the method of calculating torsional moment of inertia is accurate and effective. The one drawback to this method of calculation is the need to manually identify the separate shapes in each additional component. Further analysis would allow the study of the contribution of the wing skin to torsional stiffness, in particular, the role fibre orientation plays in increasing torsional strength.

In the building and testing of this wing model, the understanding of important engineering concepts, such as strength of materials and computer modelling, were greatly developed.

8. Annex

8.1 Physical Properties of Materials Used

Table 6: Material Properties of Materials

Material	Young's Modulus, Pa	Shear Modulus, Pa	Poisson's ratio	Density, $\frac{kg}{m^3}$
Samba	6690 x10^6		0.30	380
Spruce		71x10^6		
Balsa		181x10^6		
Plywood		209 x10^6		

8.2 Measuring Rod contribution to Torque Measurements

Table 7: Dimensions and torque of rod

Length	L	60 cm
Diameter	D	0.8 cm
Volume	V	3.0159x10^{-6} m^3
Density	ρ	7800 kg/m^3
Weight	W	2.3035 N
Centre of Gravity	CoG	30 cm
Torque	T	0.6916 Nm
Torsion Angle	∅	18° or 0.3142 rad

8.3 Solving for Beam Equivalence

8.3.1 Horizontally Aligned

The stiffness of one beam was calculated using

$$k = \frac{IE}{L}$$

Where

$$I = \frac{ab^3}{12}$$

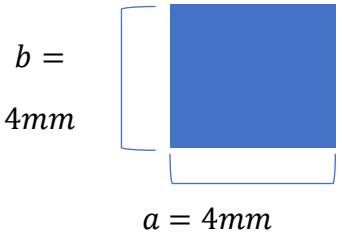

Figure 21: Dimensions of one samba beam

Geometry can be found in

Figure 21. The stiffness of one beam: $k_{\text{one beam}}$=190 Nm. The stiffness of the rib at both stages were then divided by $k_{\text{one beam}}$ to find the number of beams needed.

8.3.2 Vertically Aligned

Using

$$I = \frac{a(\boldsymbol{n} * b)^3}{12} = \frac{kE}{L}$$

The equation was solved for n, which is the number of beams aligned vertically that would produce the same stiffness.

8.4 Torsional Moment of Inertias and Analytical Torsional Angle & Stiffness

All geometry is calculated using Figure 22.

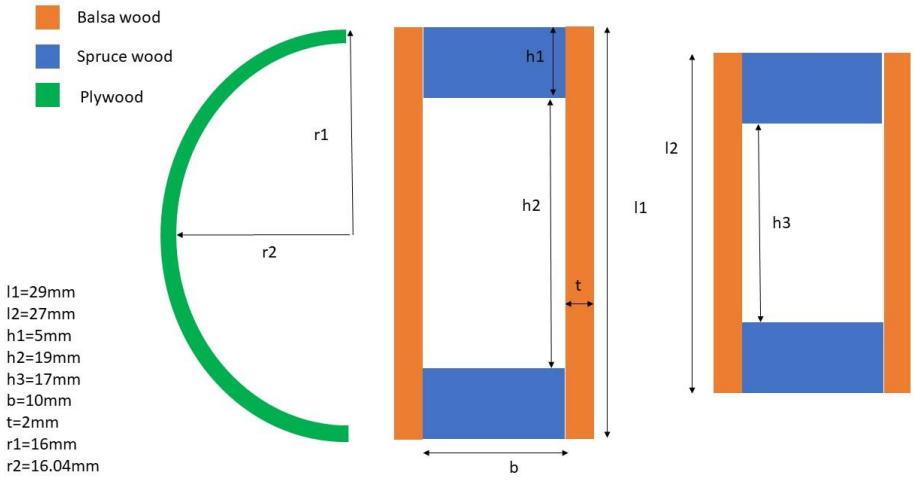

Figure 22: Geometry of structural components, a cross-section of wing

First Stage

Torsional moment of Inertia:

Spruce

Front:

$$I_x = \frac{1}{12} b {L_1}^3 - \frac{1}{12} b {h_2}^3 = \frac{1}{12} b\left({L_1}^3 - {h_2}^3\right)$$

$$I_y = \frac{1}{12} L_1 b^3 - \frac{1}{12} h_2 b^3 = \frac{1}{12} b^3 (L_1 - h_2)$$

$$J_{Spruce,Front} = \frac{1}{12} b\left({L_1}^3 - {h_2}^3\right) + \frac{1}{12} b^3 (L_1 - h_2)$$

$$J_{Spruce,Front} = \frac{1}{12} b\left({L_1}^3 - {h_2}^3 + b^2 (L_1 - h_2)\right)$$

Back:

$$I_x = \frac{1}{12} b\left({L_2}^3 - {h_3}^3\right)$$

$$I_y = \frac{1}{12} b^3 (L_2 - h_3)$$

$$J_{Spruce,Back} = \frac{1}{12} b \left({L_2}^3 - {h_3}^3 - b^2 (L_2 - h_3) \right)$$

Analytical Torsional Stiffness: $k = \frac{(J_{Spruce,Front} + J_{Spruce,Back}) G_{Spruce}}{L}$

Analytical Torsion Angle: $\emptyset = \frac{TL}{\left(J_{Spruce,Front} + J_{Spruce,Back}\right) G_{Spruce}}$

Second Stage

Torsional moment of Inertia:

Balsa

$$I_x = \frac{1}{12}(b + 2t){L_1}^3 - \frac{1}{12}(b){L_1}^3 = \frac{1}{12}(2t){L_1}^3$$

$$I_y = \frac{1}{12} L_1 (b + 2t)^3 - \frac{1}{12} L_1 b^3 = \frac{1}{12} L_1 ((b + 2t)^3 - b^3)$$

$$J_{Balsa,Front} = \frac{1}{12} L_1 \left(2t {L_1}^2 + (b + 2t)^3 - b^3\right)$$

$$J_{Balsa,Back} = \frac{1}{12} L_2 \left(2t {L_2}^2 + (b + 2t)^3 - b^3\right)$$

Analytical Torsional Stiffness: $k = \frac{\left(J_{Spruce,Front} + J_{Spruce,Back}\right) G_{Spruce} + \left(J_{Balsa,Front} + J_{Balsa,Back}\right) G_{Balsa}}{L}$

Analytical Torsion Angle: $\emptyset = \frac{TL}{\left(J_{Spruce,Front} + J_{Spruce,Back}\right) G_{Spruce} + \left(J_{Balsa,Front} + J_{Balsa,Back}\right) G_{Balsa}}$

Third Stage

Torsional moment of Inertia:

Plywood Nose

$$J_{Nose} = 2\pi R^3 t$$

Where $R = \frac{R_1 + R_2}{2}$ and $t = R_1 - R_2$.

Analytical Torsional Stiffness:

$$k = \frac{\left(J_{Spruce,Front} + J_{Spruce,Back}\right) G_{Spruce} + \left(J_{Balsa,Front} + J_{Balsa,Back}\right) G_{Balsa} + J_{Nose} G_{Plywood}}{L}$$

Analytical Torsion Angle: $\emptyset = \frac{TL}{\left(J_{Spruce,Front} + J_{Spruce,Back}\right) G_{Spruce} + \left(J_{Balsa,Front} + J_{Balsa,Back}\right) G_{Balsa} + J_{Nose} G_{Plywood}}$

8.5 CF100 analysis parameters toolbox at sea level and service ceiling

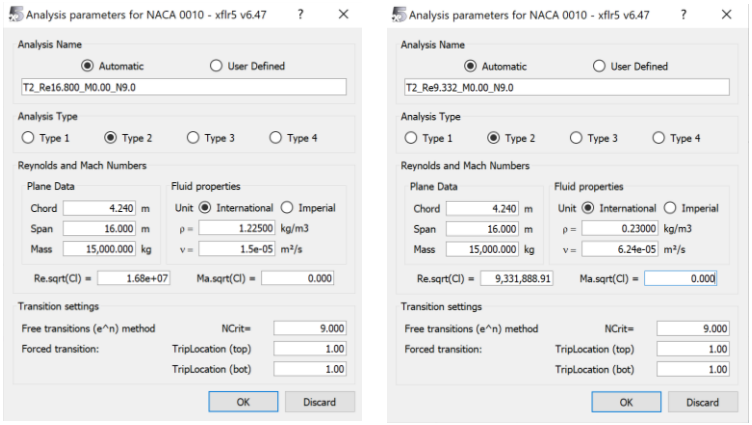

Figure 23: Analysis parameters at sea level and service ceiling

8.6 Tables and figures for the RDM6 analysis

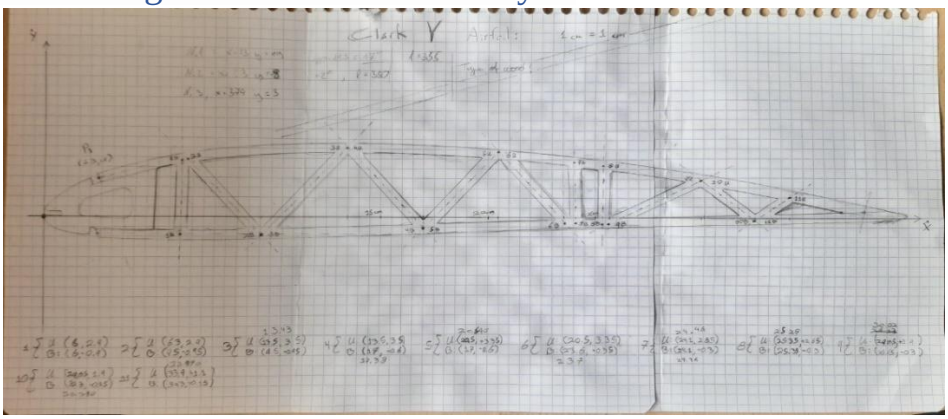

Figure 24: Real life scale drawing of wing rib

Table 8: Bottom beam and Upper beam TIP coordinates

Location number	Upper beam in the x0 direction (cm)	Upper beam in the y0 direction (cm)	Bottom beam in the x0 direction (cm)	Bottom beam in the y0 direction (cm)
1	6	2.7	6	-0.9
2	6.3	2.7	9.5	-0.95
3	13.5	3.5	9.5	-0.95
4	13.5	3.5	17	-0.6
5	20.5	3.35	17	-0.6
6	20.5	3.35	23.6	-0.35
7	24.1	2.85	24.1	-0.3
8	25.35	2.65	25.35	-0.3
9	29.85	1.9	25.65	-0.3
10	29.85	1.9	32.3	-0.15
11	33.9	1.1	32.3	-0.15

Description on how alpha was measured:

The coordinates chosen to calculate the angle made between the bent wing rib and a straight upper beam are:

P1(3.95 cm x0, 2.4884 y0), P2(4.74 cm x0, 2.7105 cm y0)

Alpha can be obtained by doing some simple trigonometry as these two points can be considered to form part of a right-angle triangle.

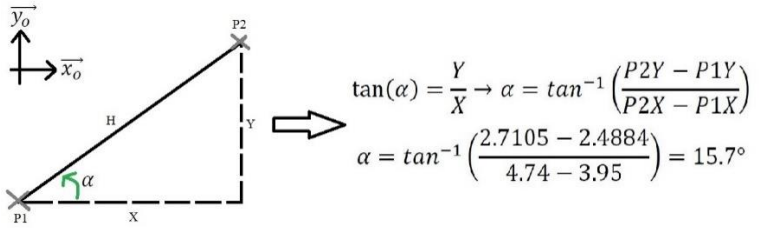

Figure 25: Right-angle triangle used to obtain alpha

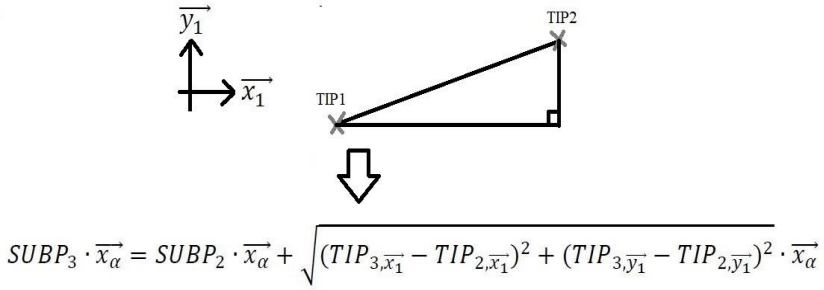

Figure 26: Example of how to obtain an SUBP

Table 9: TIP and SUBP coordinates and delta y1-8

TIP in the $\overrightarrow{x_1}$ direction (cm)	TIP in the $\overrightarrow{y_1}$ direction (cm)	SUBP in the $\overrightarrow{x_\alpha}$ alpha direction (cm)	SUBP in the $\overrightarrow{x_1}$ direction (cm)	SUBP in the $\overrightarrow{y_1}$ direction (cm)	δ_y in the $\overrightarrow{y_1}$ direction (cm)
1.5	0.360	1.5	1.444	0.406	-0.046
8.7	0.915	7.525	7.244	2.036	-1.122
15.7	0.630	14.527	13.985	3.931	-3.302
19.3	0.242	18.161	17.483	4.915	-4.673
20.55	0.074	19.427	18.702	5.257	-5.184
25.05	-0.646	23.989	23.094	6.492	-7.138
29.1	-1.423	28.117	27.068	7.609	-9.032
-32.69	-2.205	31.795	30.609	8.605	-10.810

$$\begin{bmatrix} \frac{F_1 \cdot SUBP_1{}^3}{3 \cdot E \cdot I} & \cdots & \frac{F_8 \cdot SUBP_1{}^2}{6 \cdot E \cdot I}(3 \cdot SUBP_8 - SUBP_1) \\ \vdots & \ddots & \vdots \\ \frac{F_1 \cdot SUBP_8{}^2}{6 \cdot E \cdot I}(3 \cdot SUBP_1 - SUBP_8) & \cdots & \frac{F_8 \cdot SUBP_8{}^3}{3 \cdot E \cdot I} \end{bmatrix} = \begin{bmatrix} \delta_{y1} \\ \vdots \\ \delta_{y8} \end{bmatrix}$$

Figure 27: 8 by 8 matrix of cantilever beam super-positioning of deflections

Table 10: Forces obtained from the MATLAB code: Clark-Y wing rib calculations

F in the $\overrightarrow{y_\alpha}$ direction (N)	F in the $\overrightarrow{x_1}$ direction (N)	F in the $\overrightarrow{y_1}$ direction (N)
19.625	-5.311	18.893
-7.030	1.902	-6.767
-0.362	0.098	-0.348
0.008	-0.002	0.008
0.462	-0.125	0.445
-1.647	0.446	-1.585
3.688	-0.998	3.550
-3.128	0.846	-3.011

Table 11: Values of delta y, dy and the percentage error between them

δ_y in the $\overrightarrow{y_1}$ direction (cm)	dy in the $\overrightarrow{y_1}$ direction (cm)	Percentage error
-0.04603	-0.046	0.021 %
-1.1215	-1.121	0.042 %
-3.3015	-3.301	0.014 %
-4.6734	-4.672	0.029 %
-5.1835	-5.182	0.028 %
-7.1376	-7.136	0.022 %
-9.032	-9.03	0.022 %
-10.81	-10.8	0.091 %

9. References

[1] "Wikipedia," [Online]. Available: https://en.wikipedia.org/wiki/Avro_Canada_CF-100_Canuck.

[2] A. Gopalarathnam, "What is reduced Reynolds number?," [Online]. Available: http://www.krnet.org/as504x/reduced_re.html.

[3] "CLARK Y AIRFOIL," Airfoil Tools, 2020. [Online]. Available: http://airfoiltools.com/airfoil/details?airfoil=clarky-il. [Accessed 10 10 2020].

[4] "gradeup," [Online]. Available: https://gradeup.co/deflection-of-beams-study-notes-for-civil-engineering-i-6c9c3b70-84d8-11e7-ae2c-861c95b99029.